JOURNAL OF THERMOPHYSICS AND HEAT TRANSFER
Vol. 20, No. 1, January–March 2006

Direct Measurements of Eddy Transport and Thermal Dispersion in High-Porosity Matrix

Yi Niu* and Terry Simon†
University of Minnesota, Minneapolis, Minnesota 55455
David Gedeon‡
Gedeon Associates, Athens, Ohio 45701
and
Mounir Ibrahim§
Cleveland State University, Cleveland, Ohio 44115

Thermal losses from hot to cold ends of a Stirling cycle regenerator as a result of streamwise conduction and thermal dispersion in the matrix significantly degrade performance. Cross-stream conduction and thermal dispersion aids in reducing inlet flow and temperature nonuniformities. Thus, quantification of conduction and thermal dispersion is important for design. Thermal dispersion can be divided into a flow-driven eddy dispersion component, and, in the flow direction, a flow-driven advection dispersion component. Because regenerator design choices affect the components differently, it is advantageous to evaluate them separately. The focus of this paper is the measurement of the eddy component of dispersion. This component is caused by mixing within the pores by eddies created by flow separation off the solid-phase elements. Because of poor access to void spaces within a porous medium, no direct measurements have been made, and eddy dispersion models have been derived indirectly. In the current program, a large-scale porous matrix consisting of stacked wire screens with a porosity of 90% is installed in a flow rig, which is operated at an engine-representative Reynolds number. Measurements are made of eddy transport of momentum normal to the flow direction at the exit plane of the matrix using multiple hot-film sensors. The relationship of such a turbulent transport term to cross-stream and streamwise eddy thermal dispersion in the volumetric-averaged energy equation for the regenerator matrix is developed. An eddy dispersion model based upon a coefficient from the measurements and the functional form of the Prandtl mixing length model is proposed. This correlation agrees with several in the literature. Such agreement supports this measurement method.

Nomenclature

C_p = specific heat of fluid phase, J/kg K
C_t = correlation coefficient
d = characteristic length, m
d_h = hydraulic diameter, m
K = permeability of porous matrix, m^2
$\boldsymbol{k}_d$ = thermal dispersion conductivity, W/mK
k_f = thermal conductivity of fluid phase, W/mK
N = number of points selected to evaluate eddy viscosity
Pe = Peclet number $= ud_h/\alpha_f$
Re = Reynolds number, $= U_D d_h/\nu_f$
r = radial locations, m
T = temperature, K
U_D = Darcy velocity, m/s
u = velocity, m/s
α_f = thermal diffusivity of fluid phase, m^2/s
ε_d = thermal dispersion eddy diffusivity, m^2/s
ε_M = eddy diffusivity of momentum, m^2/s
$\boldsymbol{\lambda}$ = dispersion coefficient
ρ = density of fluid phase, kg/m^3
σ = anisotropy factor

Presented as Paper 2004-5646 at the International Energy Conversion Engineering Conference, Providence, RI, 16–19 August 2004; received 9 November 2004; revision received 3 March 2005; accepted for publication 9 March 2005.

*Research Assistant, Department of Mechanical Engineering, 111 Church Street SE. Member AIAA.
†Professor, Department of Mechanical Engineering, 111 Church Street SE. Member AIAA.
‡Consultant, Gedeon Associates, 16922 South Canaan Road. Member AIAA.
§Professor, Department of Mechanical Engineering, 1960 East 24th Street. Associate Fellow AIAA.

Introduction

POROUS materials have been widely used for regeneration of engines, such as Stirling engines. Typically, Stirling engine regenerators are made of wire screens or random fibers. The regenerator allows the ideal Stirling cycle machine to have a cycle efficiency equal to the Carnot cycle efficiency. Regenerator flow losses and heat transfer through the matrix contribute significantly to degrade the performance of the Stirling cycle, however. An important degradation mode is via the net energy flux through the regenerators directly to the coolers.[1] A 1% decrease in energy storage in an engine regenerator matrix might necessitate a $4 \sim 5\%$ increase in thermal energy input to a heater (i.e., a $4 \sim 5\%$ decrease in efficiency), assuming the same indicated power. A major contribution to this energy transfer has become known as enhancement in axial heat conduction as a result of dispersion within the working gas (a component of which is caused by eddy diffusion). It is a result of interaction of the flow with the regenerator matrix. Another degradation of the regenerator comes from introducing the flow to the regenerator inlet nonuniformly. Cross transport of momentum and thermal energy by eddy dispersion can lead to an evening of those nonuniformities.

In porous media, "dispersion" is described as "heat transfer due to hydrodynamic mixing of the interstitial fluid at the pore scale."[2] It can be derived from the energy equation using volume-averaging techniques and is defined as a correlation of the spatial fluctuations of temperature and velocity. For a flow with a high Peclet number, the thermal dispersion conductivity tensor $\boldsymbol{k}_d$ can be modeled as

$$\boldsymbol{k}_d = \boldsymbol{\lambda} k_f Pe \tag{1}$$

The dimensionless parameter $\boldsymbol{\lambda}$ depends on the structure of the porous medium, the flow structure, and the flow direction. However, for a homogeneous isotropic porous matrix, the component of thermal dispersion as a result of eddy transport might be isotropic. It can be a main contributor of thermal dispersion in the cross-stream direction. The eddy component of dispersion is the focus of the present paper.

Extensive investigations have experimentally and theoretically determined the dispersion coefficient. Most of the research has focused on packed-particle beds, which simulate many of the porous media in nature. For this type of porous medium, Yagi and Kunni[3] determined the coefficient λ equal to $0.09 \sim 0.1$. Hsu and Cheng[4] carried out experiments in cylindrical and annular tubes filled with glass spheres and derived the radial dispersion coefficient as a function of porosity. More recently, the radial dispersion coefficient for packed beds was determined by Metzger et al.[5] to be about 0.03. They used the particle diameter d as the characteristic length.

The porous structures of Stirling regenerators (consisting of wire screen or random fibers) differ from those for a packed bed. Moreover, the Stirling engine regenerators have a high porosity ($80 \sim 95\%$) compared to packed beds (less than 40%). Therefore, none of the preceding models should be used directly in Stirling regenerators. Koch and Brady[6] analytically derived models for fibrous media. They gave different expressions for different flow regimes and different directions, though the functional form of the expressions was common. Nakayama and Kuwahara[7] numerically modeled convective heat transfer through a number of square rods as microscopic structures of a porous medium and gave correlations of dispersion in both longitudinal and transverse directions. Both models include the porosity as a parameter. Hunt and Tien[8] measured heat transfer through a wall to porous media with porosities up to 97% and determined dispersion coefficients in that region to be about 0.025. They used the square root of the permeability $\sqrt{K}$ as the characteristic length. Few researchers have addressed modeling of dispersion in Stirling machines. Gedeon and Wood[9] extracted axial transport rates from experiments taken under oscillatory flow conditions. Results were derived from the cycle average temperature gradient of the regenerator and the net regenerator energy flux. They derived correlations of effective axial conductivity for various porous structures commonly used in Stirling cycle regenerators.[9,10]

Kaviany[11] summarized different experimental methods for determining thermal dispersion. The experimental methods frequently used (e.g., Refs. 5 and 8) require a solution of the macroscopic energy equation with the thermal dispersion coefficient included as a parameter. One can obtain the dispersion coefficient by matching the measured temperatures or the measured heat-transfer coefficients to those predicted by the solution. To the authors' knowledge, no efforts have been taken to assess thermal dispersion by measuring flow velocity and temperature at the pore level, directly. There exist two challenges. One is that the complex geometries of typical porous media prevent access by existing probes. Even if access were gained, the evaluation of spatial correlations of flow and temperature fields requires a number of probes within the porous medium so that the readings can be taken simultaneously. This does not seem practical. The present paper is attempting to evaluate the eddy component of dispersion by direct measurements at the exit plane of the medium. The spatial variations of the velocity and temperature fields are described in terms of temporal variations with the aid of the following theoretical approach.

Theoretical Approach

A volume-averaging technique has been commonly used in porous media studies. Any microscopic quantity W can be decomposed into the sum of the volumetric-average (macroscopic) quantity $\langle W \rangle$ integrated over a representative elementary volume (R.E.V.) and a spatial variation $\tilde{W}$:

$$W = \langle W \rangle + \tilde{W} \tag{2}$$

where W and $\tilde{W}$ are functions of both time and space and $\langle W \rangle$ is a function of time, only. One can obtain one single volume-averaged energy equation by applying this technique to the energy equations for both solid and fluid phases while assuming thermal equilibrium between the two phases,[4,7]

$$\rho_f C_p \langle \boldsymbol{u} \rangle \cdot \nabla \langle T \rangle = \nabla \cdot (\boldsymbol{k}_0 \nabla \langle T \rangle - \rho_f C_{\mathrm{pf}} \langle \tilde{\boldsymbol{u}} \tilde{T} \rangle) \tag{3}$$

The first term on the right side is stagnant conduction by molecular diffusion. It depends on the fluid- and solid-phase thermophysical properties, the turtuosity of the structure, and the porous medium geometry. The second term can be rewritten as

$$-\rho_f C_{\mathrm{pf}} \langle \tilde{\boldsymbol{u}} \tilde{T} \rangle \equiv \boldsymbol{k}_d \cdot \nabla \langle T \rangle \tag{4}$$

Here, the tensor $\boldsymbol{k}_d$ is called the flow-driven thermal dispersion conductivity. Correspondingly, flow-driven thermal dispersion diffusivity for axial transport is defined as

$$\varepsilon_d = \frac{k_d}{\rho_f C_{\mathrm{pf}}} \equiv -\frac{\langle \tilde{u} \tilde{T} \rangle}{\partial \langle T \rangle / \partial x} \tag{5}$$

It can be seen that the axial thermal dispersion diffusivity ε_d is the spatial average of the correlation between spatial variations of temperature and velocity divided by the gradient of the spatial average temperature in the axial direction.

To obtain this correlation, one can choose an R.E.V., locate with a high spatial resolution a number of probes for temperature and velocity measurements within it, then take their readings, simultaneously. Afterwards, one can calculate the spatial-averaged quantities over the R.E.V. at any instant in time and the spatial variations at any instant in time and at any particular location. The needed term $\langle \tilde{u} \tilde{T} \rangle$ is computed by spatially averaging $\tilde{u} \tilde{T}$. However, this proposed experimental method cannot be realized.

In contrast to the spatial average technique used in porous media is the evaluation of turbulence quantities taken in free and wall-bounded flows (but not porous media) in which a time average is used to characterize the turbulence field. Any quantity can also be defined as the sum of the time-averaged value integrated over a time period that is sufficiently large relative to the characteristic timescale of the fluid flow within the pore and a temporal fluctuation value.

$$W = \bar{W} + W' \tag{6}$$

W' is a function of time and space, and $\bar{W}$ is a function of space, only.

These time-averaged quantities can be measured for an open flow by locating a probe at individual points in space and recording the readings continuously in time. This type of measurement is frequently taken. This raises the question, "Is it possible to use time-averaged values to describe the needed volumetric-averaged values?" We note that the time-averaged values we will use for modeling are to be volume averaged over a representative area of regenerator matrix. Also, the volume-averaged values used for characterizing porous media are actually time averaged because they are used in steady flow or quasi-steady flow models. Efforts have been taken to make a connection mathematically between volumetric-averaged quantities and time-averaged quantities.[12] Combining Eqs. (2) and (6) allows writing the volumetric-averaged value $\langle W \rangle$, decomposed into the volumetric average of the time averages and the temporal fluctuation terms as follows:

$$\langle W \rangle = \langle \bar{W} + W' \rangle = \langle \bar{W} \rangle + \langle W' \rangle \tag{7}$$

where $\langle W' \rangle$ can be a function of time. However, the temporal variation of $\langle W' \rangle$ would be small if the times and volumes for averaging are large enough relative to turbulent eddy passing timescales and turbulence length scales, respectively. The spatial variation of any quantity $\tilde{W}$ can be written as

$$\tilde{W} = W - \langle W \rangle = \bar{W} + W' - (\langle \bar{W} \rangle + \langle W' \rangle) \approx \bar{W} - \langle \bar{W} \rangle + W' \tag{8}$$

For the spatial variations at individual spatial points, it is assumed that time and space averaging is commutative. We note that $\langle W \rangle$ is an average of W over the R. E. V. It could change with time

because it is influenced by the passing eddies; but, because it is a space-averaged value, it is expected to be essentially time invariant.

Applying Eq. (8) to velocity and temperature components of the fluid phase, and then applying the volume-averaging technique to obtain the volumetric average of the product of $\tilde{u}$ and $\tilde{T}$ inside the porous medium, one can have

$$\langle \tilde{u}\tilde{T} \rangle = \langle (\bar{u} - \langle \bar{u} \rangle + u')(\bar{T} - \langle \bar{T} \rangle + T') \rangle$$
$$= \langle \bar{u}\bar{T} \rangle - \langle \bar{u} \rangle \langle \bar{T} \rangle + \langle \bar{u}T' \rangle + \langle u'\bar{T} \rangle + \langle u'T' \rangle \quad (9)$$

The first and second terms can be calculated from single-point experimental measurements because they do not require simultaneous measurements. In most applications, instead of $\langle \tilde{u}\tilde{T} \rangle$, $\langle \tilde{u}\tilde{T} \rangle$ is of interest. The overbar represents an average over a period that is sufficiently long to capture all eddy scales of importance. If one can apply the time averaging to Eq. (9), the third and forth terms go to zero. Then $\langle \tilde{u}\tilde{T} \rangle$ is reduced to the sum of three terms,

$$\overline{\langle \tilde{u}\tilde{T} \rangle} = \langle \bar{u}\bar{T} \rangle - \langle \bar{u} \rangle \langle \bar{T} \rangle + \overline{\langle u'T' \rangle} \quad (10a)$$

Similarly, for the cross-transport thermal energy transport and momentum transport,

$$\overline{\langle \tilde{v}\tilde{T} \rangle} = \langle \bar{v}\bar{T} \rangle - \langle \bar{v} \rangle \langle \bar{T} \rangle + \overline{\langle v'T' \rangle} \quad (10b)$$

$$\overline{\langle \tilde{u}\tilde{v} \rangle} = \langle \overline{uv} \rangle - \langle \bar{u} \rangle \langle \bar{v} \rangle + \overline{\langle u'v' \rangle} \quad (10c)$$

Because we are interested in the eddy transport component and believe that it is a main contributor to cross-stream dispersion, we now focus on the cross-stream transport. As the first stage of our study, we now use the momentum transport results [Eq. (10c)] to discuss thermal transport [Eq. (10b)] by imposing Reynolds analogy, which states that momentum and thermal eddy diffusivities are nearly equal. This is commonly applied in the modeling of eddy transport and is robust in flow such as this so long as the molecular Prandtl number is of the order of unity. Thus, with this assumption of analogous behavior between momentum and thermal eddy transport, we assume a turbulent Prandtl number of unity.

Because the effect of eddy transport is often dominant in cross-stream dispersion, knowing the eddy transport term of cross-stream dispersion is valuable. The three terms on the right can be measured. The Appendix shows that the sum of the second and third terms is small, relative to the third term. The equation is therefore reduced to measuring $\overline{\langle u'v' \rangle}$ within the porous matrix, or $\langle \overline{u'v'} \rangle$, because the spatial and temporal averages are interchangeable. Then, Eq. (10c) allows saying,

$$\overline{\langle \tilde{u}\tilde{v} \rangle} \approx \overline{\langle u'v' \rangle} = \langle \overline{u'v'} \rangle \quad (11)$$

Recognizing the difficulty of measuring $\langle \overline{u'v'} \rangle$ within the matrix, one might ask "Can the measurements be done within the turbulence structure of the flow just exiting the matrix instead of within the matrix?" Turbulent flows within porous media are different from free turbulent flows or turbulent flows far downstream of porous media. In the case of free turbulent flows, eddies are formed as a breakdown of a shear layer. The eddies then strain one another according to the turbulence cascade theory. In porous media, the eddies are generated continuously because of separation off local solid surfaces. In some respects, this is similar to near-wall boundary-layer turbulence where production of turbulence by inner-layer instabilities continuously produces turbulent eddies. A probe located within the porous medium (or a boundary layer) not only sees the decaying eddies left over from upstream, but also eddies produced locally that might have a large contribution to the eddy transport. Little research has been done on presenting a physical explanation of turbulent eddy transport in porous media. Masuoka and Takatsu[13] provided the most detailed description of transport through porous media in terms of vortex transport. They categorized two types of vortices formed within porous media: void vortices and pseudovortices. They noted that pseudovortices are the main contributors to thermal dispersion in that they play the role of long-distance (large-scale) momentum transport. We expect that they have a lifetime of at least several eddy turnovers.

Because the pseudovortex has a large scale and some longevity, it might be measured immediately downstream of the porous medium instead of within the porous medium. This is similar to the assumption of advected "frozen turbulence" in which the turbulence field is unchanged as it exits the matrix and is advected downstream. One still can capture a major contribution of dispersion caused by eddy transport. As the scale of the pseudovortex might increase with the porosity, this statement becomes stronger as we approach the high-porosity values seen in Stirling engine regenerators.

Experimental Measurements

Experimental Setup

The porous medium in the present test is a simulation of a Stirling engine regenerator matrix operating under representative flow conditions. It consists of 200 round layers of 6.3×6.3 mm square mesh (four mesh per inch), stainless steel 304, welded screens. Each layer is a disk of 190 mm diam. The wire diameter d_w of the screens is 0.81 mm. The screens are stacked in such a way that each layer is rotated 45 deg from the adjacent layer to simulate random wire arrangement of the real Stirling regenerator. The axial spacing of the screens is such that the regenerator has 90% porosity. The screen is punched out of welded screen sheets in such a way that the location of the center of the disc is random with respect to the center of the mesh in which it resides, adding to the randomness of the matrix. The permeability of the stacked regenerator matrix is 1.86×10^{-7} m^2. A more detailed description of the porous matrix is given in Ref. 14. A summary of important geometric parameters is given in Table 1. Under unidirectional, steady flow operation, air at room temperature and pressure is introduced to the regenerator matrix through a duct of 2600 mm length and a diameter that matches the disk diameter of 190 mm. The flow in this duct is well mixed so that the velocity distribution of the entry flow is flat. A triple-sensor, hot-film anemometer probe (TSI 1299BM-20) is located downstream of the regenerator matrix exit plane. This probe has been qualified in a fully developed turbulent pipe flow. In this qualification test, we verified that we can accurately measure turbulent shear stresses in a flow with a smaller Taylor microscale (8 mm) and associated timescale (1 ms) than in the exit flow of the matrix, 10 mm and 7 ms, respectively. The experimental setup for the matrix flow measurements is described in Fig. 1. Three velocity components u, v, and w were measured, for various radial positions from -38 to 38 mm (± 1.5 in.) about 0.0, which is the radial center of the matrix. A sampling frequency of 10 kHz is used. By doing so, the turbulent shear stress $\overline{u'v'}$ can be evaluated. To create a radial velocity gradient $\partial \bar{u}/\partial r$ and a nonzero $\overline{u'v'}$, a plate with a 12.5-mm (0.5-in.)-diam orifice in the middle is

Table 1 Geometry of the porous medium and operating conditions

Parameter	Value
Wire diameter, mm	0.8
Mesh size, PPI	4×4
Hydraulic diameter, mm	7.2
Porosity	90%
Darcy velocity U_D, m/s	~ 1.5
$Re = U_D d_h / \nu_f$	~ 680

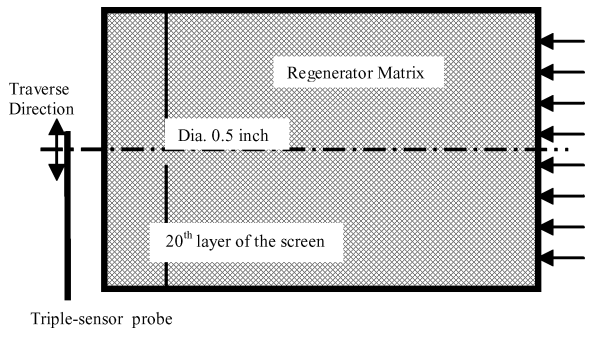

Fig. 1 Experimental setup for turbulent transport measurements.

inserted into the regenerator at the 20th layer of screen from the exit plane. As a result, local radial eddy diffusivity of momentum can be obtained as

$$\varepsilon_M(r_i) = \frac{-\overline{u'v'}}{\partial u/\partial r} \tag{12}$$

where $-\overline{u'v'}$ and $\partial u/\partial r$ vary with position r.

Data Processing and Results

Figure 2a shows a velocity profile at an axial location of 3.2 mm (0.125 in.) away from the exit plane of the regenerator. Because of the irregularity of the regenerator matrix, the probe might be located immediately behind a wire or immediately behind a pore. Therefore, the velocity distribution is highly variable in the radial direction, which makes it difficult to accurately evaluate the local, radial velocity gradients and the shear stress $\overline{u'v'}$. To avoid this situation attributed to the close proximity to the mesh wires, the probe is moved further away from the exit plane. The velocity profiles from 3.2 mm (0.125 in.) to 50.8 mm (2.0 in.) are shown in Fig. 2. It can be seen that the radial distribution of velocity is becoming much smoother, ensuring a more accurate evaluation of the local radial velocity gradient and shear stress $\overline{u'v'}$. We were surprised to see that the profile developed a double bump, though it had passed through a single orifice hole 20 screen layers upstream. The reason remains unknown but it may be associated with the nonlinear flow resistance of the jetting flow through porous materials. The orifice plate created a mean shear in the flow, however, which was its sole purpose.

We might expect that eddy transport in the measurement zone might differ from that immediately behind the exit plane. With all of the information at the various axial locations, we are tempted to assume that the turbulent structure does not change too much within a short distance downstream of the exit plane. To check the suitability of doing this, we seek a relationship between the eddy diffusivity and the axial distance from the exit plane, as $\varepsilon_M = \varepsilon_M(x)$. To eliminate the effect of randomness, only points with smooth gradients are chosen for evaluation of the averaged eddy diffusivity $\langle \varepsilon_M \rangle$ at each axial location,

$$\langle \varepsilon_M \rangle \approx \sum_{r_i} \frac{\varepsilon_M(r_i)}{N} \tag{13}$$

The radial line average $\langle\ \rangle$ is taken. Because the matrix is random, this represents any line, area, or volume average. The parameter N is the number of selected points for data processing, indicated in Fig. 2 as points with symbols in solid circles. As an example, the velocities at the axial location 50.8 mm (2 in.) away from the exit plane are

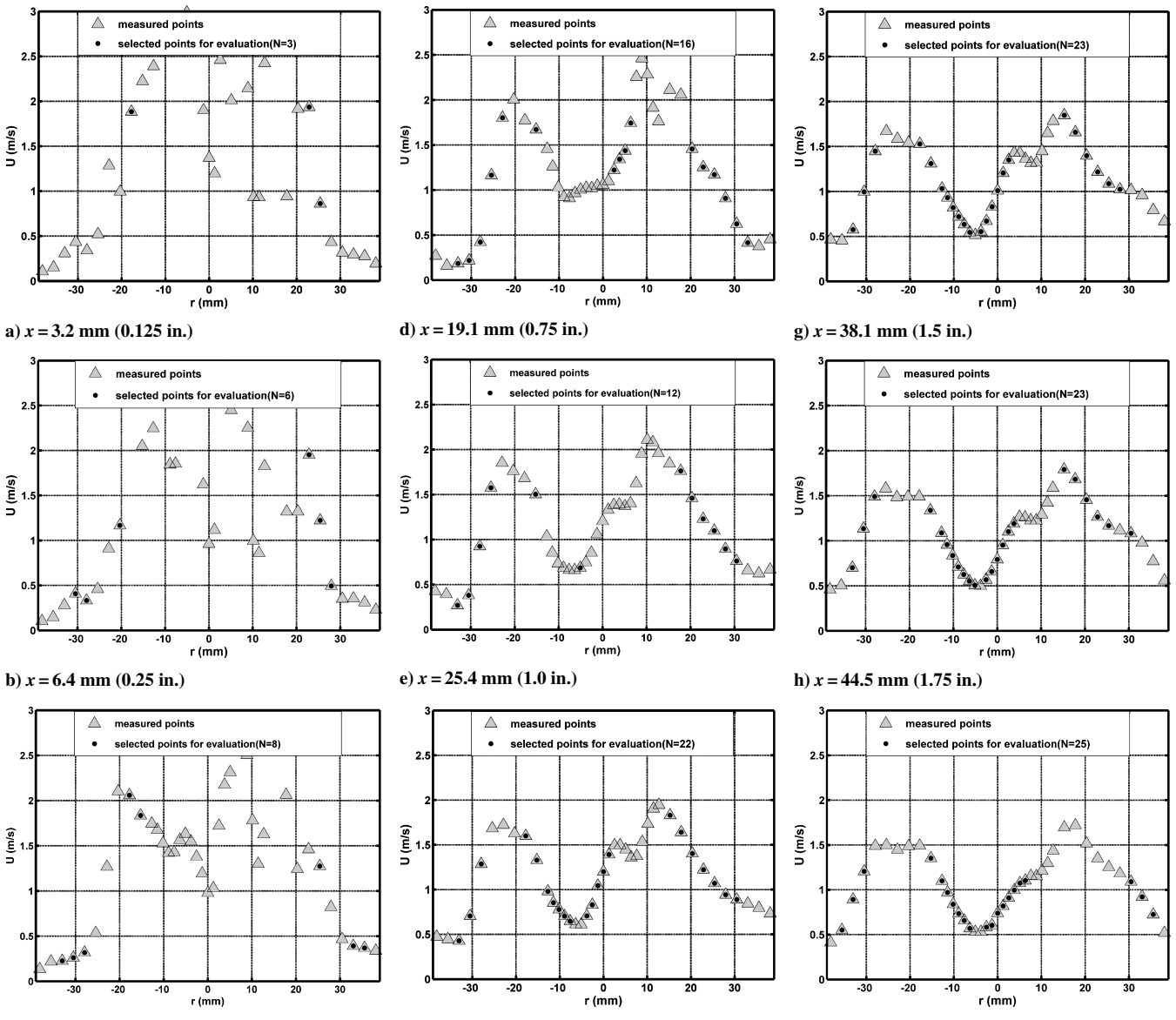

a) $x = 3.2$ mm (0.125 in.) d) $x = 19.1$ mm (0.75 in.) g) $x = 38.1$ mm (1.5 in.)

b) $x = 6.4$ mm (0.25 in.) e) $x = 25.4$ mm (1.0 in.) h) $x = 44.5$ mm (1.75 in.)

c) $x = 12.7$ mm (0.5 in.) f) $x = 31.8$ mm (1.25 in.) i) $x = 50.8$ mm (2 in.)

Fig. 2 Velocity distribution at various axial locations.

plotted in Fig. 2i). In this case, 28 points are considered to be the points with smooth velocity gradients. Points with weak gradients were not processed. We find that several of the neighboring points to those eliminated (caused by a weak gradient) show measured shear-stress values that are of the wrong sign relative to the local mean shear, giving a negative eddy diffusivity. We consider those points erroneous as well because, we suppose, we are not able to capture the relevant length scales of the Reynolds shear stress $\overline{u'v'}$. Points that are well inside of a continuous mean shear gradient region pass both of these tests and are processed. The direction of mean shear is not important to the processing. After these points have been eliminated, the number of selected points for evaluating the averaged values N is equal to 25. These are solid circles in Fig. 2i. By similarly processing data at the other planes in Fig. 2, we can see that the number of points processed decreases significantly as the measurement plane becomes closer to the matrix exit plane. We will see also that the data scatter correspondingly.

To derive a model, we use the Prandtl mixing length hypothesis to compute the eddy diffusivity as the product of a characteristic length (taken to be the hydraulic diameter) and a characteristic velocity (taken to be the in-matrix average velocity),

$$\varepsilon_M(r_i) = \lambda d_h U \tag{14}$$

We will see that this gives a dispersion model that is of the same form as those in the literature. An average diffusivity coefficient is defined as

$$\langle\lambda\rangle \approx \sum_{r_i} \frac{(\varepsilon_M(r_i)/d_h U)}{N} \tag{15}$$

We perform this average by processing points along a radius. Figures 3a and 3b indicate the values of $\langle\varepsilon_M\rangle$ and $\langle\lambda\rangle$, respectively, for various axial locations. Because U changes across the measurement plane, we find that $\langle\varepsilon_M\rangle$ data scatter from plane to plane more than $\langle\lambda\rangle$ scatters. This supports the application of Eq. (14), a model that seems to capture this velocity effect.

The flow we have been measuring is that which is emerging from between the wires of the matrix. It has some characteristics of free-jets. Measurements by others of eddy transport indicate that the eddy diffusivity remains invariant with axial position for the near field of axisymmetric freejets. If the present case could be modeled as an array of freejets, we might be inclined to assume that $\langle\varepsilon_M\rangle$ is invariant with axial position and extract from Fig. 3a a constant eddy diffusivity of around $1.7 \times 10^{-4}\text{m}^2/\text{s}^2$ and from Fig. 3b a corresponding coefficient $\langle\lambda\rangle$ of 0.02. The scatter in values of $\langle\lambda\rangle$ would indicate an uncertainty of about 25%. In choosing the values and the uncertainty, we put low emphasis on the three planes nearest the regenerator exit because so few of the measurements pass the two acceptance criteria just described.

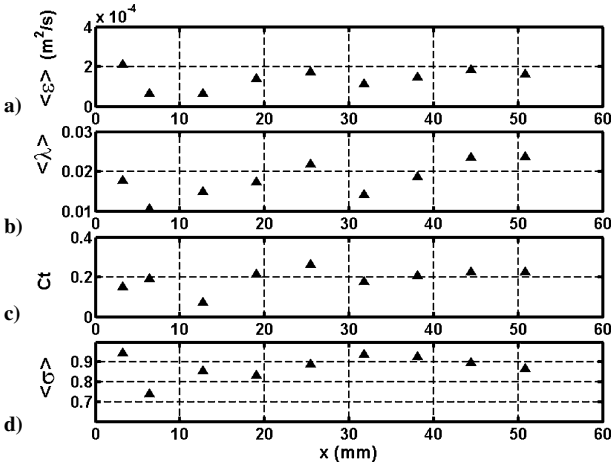

Fig. 3 Values calculated by Eqs. (13), (15), (16), and (17).

We next test the hypothesis that the structure does not change within the measurement zone. To test this assumption with our measured data, we define a correlation coefficient C_t and an anisotropy factor σ as follows:

$$\langle\overline{u'v'}\rangle = C_t\langle\sqrt{\overline{u'^2}}\rangle\langle\sqrt{\overline{v'^2}}\rangle \tag{16}$$

$$\sigma = \sqrt{\overline{v'^2}}\Big/\sqrt{\overline{u'^2}} \tag{17}$$

If the flow structure does not change within the measurement zone, we might expect that values for these two are invariant with x. If so, the experiment could be reduced to measuring the correlation coefficient and the anisotropy factor in the exit stream, and only the intensity value $\sqrt{u'^2}$ within the matrix or at the exit plane of the matrix.

$$\langle\overline{u'v'}\rangle = C_t\sigma\langle\overline{u'^2}\rangle \tag{18}$$

The correlation coefficient and the anisotropy factor are computed for each x plane. Radius-average values at each axial position using the selected points are substituted for volume averages in doing this evaluation (see Figs. 3c and 3d). This $C_t(x)$ is extrapolated to the $x = 0$ position to give about 0.2, again with reduced emphasis on the three measurement planes nearest the matrix. It is observed that a value of 0.9 for σ is maintained along the streamwise direction. This supports our preceding assumption that the turbulence structure does not change in this 50 mm length (again, advected frozen turbulence). With this assumption, we return to Fig. 3b to extract a value of $\lambda = 0.02$ from the data.

Discussion

From the current experimental measurements, a model is suggested for evaluating the eddy transport component of the cross-stream dispersion in stacked wire screens or similar porous structures. It is Eq. (14) with $\boldsymbol{\lambda} = 0.02$.

$$\varepsilon_M = 0.02 d_h U \tag{19}$$

Alternatively, a model for the eddy component of thermal dispersion conductivity as a function of the Peclet number can be assigned by use of, Reynolds analogy, $\varepsilon_H = \varepsilon_M$, and the definitions, $\varepsilon_H = k_d/\rho C_p$, and $Pe = u d_h/\alpha_f$,

$$k_d = 0.02 k_f Pe \tag{20}$$

A comparison of the models by different researchers is given in Table 2. Because these models employ different forms and different length scales, for the purpose of comparison, all dispersion coefficients are computed based upon the hydraulic diameter of the current porous medium and local in-pore velocity (given in Table 1).

It can be seen that the thermal dispersion coefficients scatter widely, even for the similar porous materials. We note, however, that the modeled conditions differ from case to case, as will now be discussed.

The theoretical model given by Koch and Brady[6] was derived from an isotropic packed fibrous media, which is the best presentation of the porous matrix in the present study. The model by Nakayama and Kuwahara[7] was developed from numerical simulations using a microscopic structure of square rods. All of the rods in their structure are in-line and perpendicular to the flow direction, which is similar to the aligned fibers studied by Koch and Brady[6]

Table 2 Comparison of the thermal dispersion coefficients

Researchers	Models	Porous media
Current researchers	$k_d = 0.02 k_f Pe$	Welded screen
Koch and Brady[6]	$k_d = 0.024 k_f Pe$	Isotropic fibers
Koch and Brady[6]	$k_d = 0.0004 k_f Pe$	Aligned fibers
Nakayama and Kuwahara[7]	$k_d = 0.0018 k_f Pe$	Square rods
Hunt and Tien[8]	$k_d = 0.0015 k_f Pe$	Fibrous media

and expected to be different than the isotropic packed fibrous structure of Koch and Brady or the wire mesh of the present study. The aligned fibers tested by Koch and Brady give a regular pattern that results in a reduced dispersion from that of the isotropic medium.

The values from the study by Hunt and Tien relate to eddy dispersion near a heated wall. We know that a wall ten region can be reduced from dispersion values which apply out in the matrix far from the wall. This might explain the smaller value than the one given by the present model.

Conclusions

An effort has been made to find a measurement technique for directly evaluating the eddy component of thermal dispersion. A relationship between thermal dispersion within a porous medium and turbulent transport in the exit flow has been discussed. The former cannot be measured with current techniques, whereas the latter can be measured in the laboratory. As a first step, eddy transport downstream of the regenerator matrix is measured at various axial locations. A model for the eddy component of cross-stream dispersion is derived from the experimental results. This model is compared to other models for evaluating thermal dispersion in porous structures. The comparison shows that the correlations scatter widely. However, we presented reasons why some might not agree with others. Agreement of the measured value with those from the correlations from the literature, which are thought to be most representative of our matrix, provide support for the measurement method proposed herein.

Appendix: Further Processing of Dispersion Terms

The three terms on the right side of Eq. (10c) are measured directly. In this Appendix, we process the data to see if the first and second terms might cancel one another or that the sum of the two is relatively small compared to the last term in Eq. (10c).

To show the relative importance between the sum of the first two terms $\langle \overline{uv} \rangle - \langle \bar{u} \rangle \langle \bar{v} \rangle$ and $\overline{\langle u'v' \rangle}$, the ratio of the two is computed and plotted in Fig. A1. The means by which the ratio was computed will now be discussed. Recall that N data points at each x location were deemed suitable for processing eddy diffusivity values. These same data points were considered for this step. For each of these N points, one neighbor on each side plus itself were taken as a representative pore size to compute the local spatial-averaged values $\langle \bar{u} \rangle$, $\langle \bar{v} \rangle$, $\langle \overline{uv} \rangle$, and $\overline{\langle u'v' \rangle}$. The points that are chosen as neighboring points might fall within the selected N points, or might not meet the selection criteria. In a case where all three points of the set meet the criteria, we declare the set to be a good data set. As an example of the processing, let us take the plane $x = 50.8$ mm. We have 15 good data sets out of the 25 points that had passed the original selection criteria. These 15 good data sets lie on three segments of radial distance over which data were taken. The three segments have the characteristic that the good data sets points are contiguous and share a mean velocity gradient of the same sign. A local average of the ratio $(\langle \overline{uv} \rangle - \langle \bar{u} \rangle \langle \bar{v} \rangle)/\overline{\langle u'v' \rangle}$ is computed for each segment. The radial average value at this x location, which is shown in Fig. A1, is computed as the average of the individual segment values.

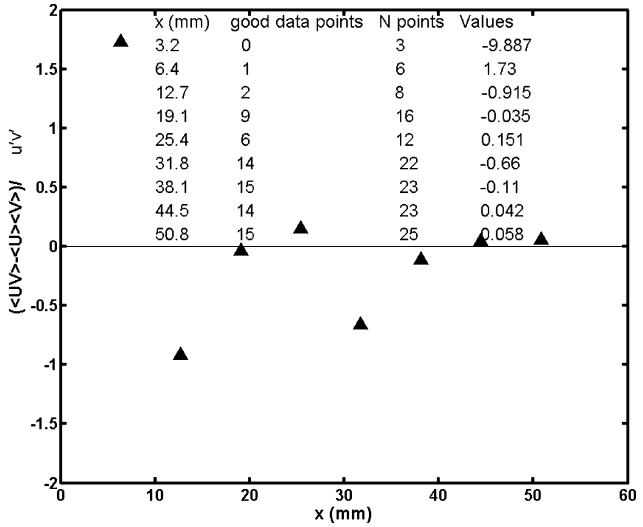

Fig. A1 $(\langle \overline{uv} \rangle - \langle \bar{u} \rangle \langle \bar{v} \rangle)/\overline{\langle u'v' \rangle}$ **at various axial locations.**

The ratio seems to be nearly zero for the x stations, where there is a sufficiently large number of good data points (further from the exit plane of the matrix). Recall that we used these stations for evaluating the other turbulence terms: λ in Eq. (15), $C_t(x)$ in Eq. (16), and σ in Eq. (17). For the first three axial locations ($x < 15$ mm) we have few good data sets, and the values scatter widely. For the remaining data, the values are much nearer zero. The last three, which have many more good data sets than those for the planes nearer the matrix, have values that scatter very little and are nearly zero. We feel that they are the most reliable data sets for this evaluation. Therefore, based on these current experimental data, we can argue that the sum of the first two terms in Eq. (10c) is small relative to the term $\langle \tilde{u}\tilde{v} \rangle$ and that the measured term $\overline{\langle u'v' \rangle}$ is approximately equal to the term $\langle \tilde{u}\tilde{v} \rangle$.

Acknowledgments

We are grateful for sponsorship of this work by the U.S. Department of Energy Office of Energy Efficiency and Renewable Energy under the Advancement of Solar Dish/Converter Technology Initiative (DE-FC36-00G010627). Also, this work was performed for NASA Headquarters, Office of Space Science (Code S) under the Project Prometheus Program and was supported by the NASA John H. Glenn Research Center under research Grant Number NNC04GA04G.

References

[1]Tew, R. C., "Overview of Heat Transfer and Fluid Flow Problem Areas Encountered in Stirling Engine Modeling," *Fluid Flow and Heat Transfer in Reciprocating Machinery*, edited by T. Morel, ASME HTD-Vol. 93, ASME, New York, 1987, pp. 77–88.

[2]Nield, D. A., and Bejan, A., *Convection in Porous Media*, 2nd ed., Springer-Verlag, New York, 1992, Chap. 2, p. 27.

[3]Yagi, S., and Kunii, D., "Studies on Axial Effective Thermal Conductivities in Packed Beds," *AIChE Journal*, Vol. 6, No. 1, 1960, pp. 543–546.

[4]Hsu, C. T., and Cheng, P., "Thermal Dispersion in a Porous Medium," *International Journal of Heat and Mass Transfer*, Vol. 33, No. 8, 1990, pp. 1587–1597.

[5]Metzger, T., Didierjean, S., and Maillet, D., "Optimal Experimental Estimation of Thermal Dispersion Coefficients in Porous Media," *International Journal of Heat and Mass Transfer*, Vol. 47, Nos. 14–16, 2004, pp. 3341–3353.

[6]Koch, D. L., and Brady, J. F., "The Effective Diffusivity of Fibrous Media," *A.I.Ch.E Journal*, Vol. 32, No. 4, 1986, pp. 575–591.

[7]Nakayama, A., and Kuwahara, F., "Numerical Modeling of Convective Heat Transfer in Porous Media Using Microscopic Structures," *Handbook of Porous Media*, edited by K. Vafai, Marcel Dekker, New York, 2000, pp. 441–488.

[8]Hunt, M. L., and Tien, C. L., "Effects of Thermal Dispersion on Forced Convection in Fibrous Media," *International Journal of Heat and Mass Transfer*, Vol. 31, No. 2, 1988, pp. 301–308.

[9]Gedeon, D., and Wood, J. G., "Oscillating-Flow Regenerator Test Rig: Hardware and Theory with Derived Corrections for Screens and Felts," NASA CR 198442, Feb. 1996.

[10]Gedeon, D., *Sage Stirling-Cycle Model-Class Reference Guide*, 3rd ed., Gedeon Associates, Athens, OH, 1999, Chap. 11.

[11]Kaviany, M., *Principles of Heat Transfer in Porous Media*, Springer-Verlag, New York, 1991, Chap. 4, pp. 217–232.

[12]Lage, J. L., Delemos, M. J. S., and Nield, D. A., "Modeling Turbulence in Porous Media," *Transport Phenomena in Porous Media II*, edited by D. B. Ingham and I. Pop, Pergamon, 2002, Chap. 8.

[13]Masuoka, T., and Takatsu, Y., "Turbulence Model for Flow Through Porous Media," *International Journal of Heat and Mass Transfer*, Vol. 39, No. 13, 1996, pp. 2803–2809.

[14]Niu, Y., Simon, T. W., Ibrahim, M., Tew, R., and Gedeon, D., "Jet Penetration into a Stirling Engine Regenerator Matrix with Various Regenerator-to-Cooler Spacings," AIAA Paper 2003-6014, Aug. 2003.